UK Atomic Energy Authority

UKAEA-STEP-PR(24)04

H Meyer, the STEP Team

Plasma Burn – Mind the Gap

Plasma Burn – Mind the Gap

H Meyer, the STEP Team

This is a preprint of a paper submitted for publication in
Philosophical Transactions A

PHILOSOPHICAL TRANSACTIONS A

Phil. Trans. R. Soc. A.
doi:10.1098/not yet assigned

Plasma Burn – Mind the Gap

H Meyer[1*] for the STEP plasma Team
[1]*UKAEA, Culham Campus, Abingdon, Oxon, OX14 3DB United Kingdom*

Keywords: spherical tokamak, burning plasma, reactor, turbulence, edge localised modes, resistive wall modes, integrated scenario modelling

Summary

The programme to design plasma scenarios for the Spherical Tokamak for Energy Production (STEP), a reactor concept aiming at net electricity production, seeks to exploit the inherent advantages of the spherical tokamak (ST) while making conservative assumptions about plasma performance. This approach is motivated by the large gap between present-day STs and future burning plasmas based on this concept. It is concluded that plasma exhaust in such a device is most likely to be manageable in a double null configuration, and that high core performance is favoured by positive triangularity plasmas with elevated central safety factor, while external heating and current drive is provided most effectively by microwaves. The gap between existing devices and STEP is most pronounced in the area of core transport, due to high normalised plasma pressure in the latter which changes qualitatively the nature of the turbulence controlling transport. Plugging this gap will require dedicated experiments, particularly on high performance STs, and the development of reduced models that faithfully represent turbulent transport at high normalised pressure. Plasma scenarios in STEP will also need to be such that edge localised modes either do not occur or are small enough to be compatible with solid material lifetime limits.

1. Introduction

The plasma is at the heart of a fusion power plant with its main function of generating the required neutrons that produce the heat for driving the turbine and breed in the blanket system tritium from lithium as part of the fuel for the deuterium tritium fusion reaction,

$$ {}^{2}_{1}\mathrm{D} + {}^{3}_{1}\mathrm{T} \rightarrow {}^{4}_{2}\mathrm{He}\ (3.5\ \mathrm{MeV}) + {}^{1}_{0}\mathrm{n}\ (14.1\ \mathrm{MeV}) \quad (1) $$

The 3.5 MeV ^{4}He nuclei (α-particles) generated in the DT fusion reaction are used to maintain the high temperature of the plasma to enable the fusion reaction to continue. A fusion power plant requires a burning plasma where the heating from the α-particles dominates over the auxiliary heating with a fusion gain $Q = \frac{P_{fus}}{P_{aux}} \gg 1$. This is needed to generate net electricity, since most of the power produced in the fusion reaction is either needed to maintain the burning plasma steady state or is lost due to inefficiency. Typically, net electricity requires a minimum $Q \sim 5 - 10$ and a commercial power plant needs $Q > 30$. The STEP prototype power plant (SPP) aims for a $Q \lesssim 10$ to produce $P_{\mathrm{net}} \sim 100$ MW with a fusion power in the range of 1.5 GW $\leq P_{\mathrm{fus}} \leq$ 1.8 GW in a device with a geometric major radius $R_{\mathrm{geo}} = 3.6$ m, aspect ratio $A = 1.8$, the toroidal field on the geometric axis $B_{t0} = 3.2\ T$, plasma current $I_{\mathrm{p}} \approx 20\mathrm{MA} - 25\mathrm{MA}$, auxiliary heating and current drive power $P_{\mathrm{HCD}} \approx 50\mathrm{MW} - 150\mathrm{MW}$ and high elongation $\kappa \approx 3$ and triangularity $\delta \approx 0.5$ in the current design iteration (1, 2). Typical parameters for a specific design point are shown in Figure 1.

To maximise the fusion yield the plasma needs to be confined for long enough at the highest possible density n_i to fulfil the extended Lawson criterion (triple product) $n_i \tau_E T_i \geq 3 \cdot 10^{21}$keV s m^{-3} where τ_E is energy confinement time (3). For typical observed scaling laws of the tokamak energy confinement time, the optimum ion temperature for break-even ($Q = 1$) $T_i \approx 15$ keV. Nested magnetic flux surfaces in a toroidal geometry provide one of the most promising concepts for confining such a hot plasma. The axisymmetric tokamak featuring a diverted plasma is the most advanced of these magnetic confinement concepts. Its cost is strongly driven by the volume and magnitude of the toroidal field B_t needed to confine a plasma with a given pressure p. The dimensionless quantity $\beta_t = 2\mu_0 \langle p \rangle / B_{t0}^2$(where angled brackets indicate volume averages), measuring the confined plasma pressure normalised to magnetic pressure, is often used as a cost indicator.

Spherical tokamaks (STs), the concept on which STEP is based, with a tight aspect ratio $1.3 \leq A = \frac{R}{a} \leq 2$ (R, a: major and minor radius of the torus) have achieved β_t values of up to 40% (4). These are about an order of magnitude higher than observed in conventional aspect ratio ($A \sim 3$) tokamaks. In addition, the small centre column enables a compact build and efficient use of the toroidal field. STs have a high natural elongation κ_{nat} and can reach high normalised beta, $\beta_N =$

*Author for correspondence (Hendrik.Meyer@ukaea.uk).

†Present address: UKAEA, Culham Campus, Abingdon, OX14 3DB, UK

$\beta_t \left(\frac{aB_t}{I_p}\right) \leq 7$ (I_p is plasma current). For example on NSTX $\kappa \lesssim 2.7$ and $\beta_N \lesssim 7$ have been observed simultaneously in the highest performing discharges (5). This makes it possible to reach high fusion power in a compact design. For a non-inductive (steady state) tokamak with high self-driven current fraction (bootstrap fraction f_{BS}) the fusion power scales like $P_{fus} \propto \frac{1}{A}(\kappa\beta_N B_t)^4$ (6). However, with respect to the Lawson criteria current STs are far from break even owing their small size and extrapolations are large. The energy confinement time observed in present day ST experiments is broadly in line with scaling laws for conventional aspect ratio tokamaks (7, 8), though scaling laws based only on ST data suggest a weaker scaling with I_{p} and a stronger scaling with B_t (9, 10) or the dimensionless quantities such as normalised collision frequency $\nu^\star$ (11, 12), safety factor q (11) and β (13). These scaling laws would extrapolate favourably to STEP but need to be treated with care due to the properties of the turbulent transport in STEP (see section 4.1).

Whilst the global plasma properties of an ST are beneficial for a reactor, the compactness of the device, in particular of the centre column, poses some key challenges for the plasma. The restricted space in the centre of the device does not allow for a sufficiently large solenoid to reach the plasma currents required for the flat-top operating point (FTOP). Therefore, non-inductive operation is mandatory for the ST even during the current ramp-up and ramp-down phases. This requires operation at high f_{BS} and efficient non-inductive current drive methods to minimise the power requirements for the auxiliary heating and current drive systems. This high $Q \lesssim 10$, high $f_{\mathrm{BS}} \lesssim 0.8 - 0.9$ operational point is a highly self-organised non-linear system that is difficult to control. Another plasma challenge is the exhaust of particles and heat through the very thin scrape-off layer (SOL) with a width of only $\lambda_{\mathrm{SOL}} \approx 1 - 2$ mm at the required plasma current and the small radius of the strike points. Hence, novel divertor concepts are needed for the plasma exhaust.

There have been several previous studies that take a low toroidal field ST as the basis for a conceptual power plant design, including STPP (14-16), ST pilot plants and FNSF (6, 17), ARIES-ST (18) and VECTOR (19, 20), or use the option of high toroidal field in an ST (21), with aspect ratios in the range $1.4 \leq A \leq 2$. The plasma parameters for these designs, aiming for very compact solutions, sometimes with resistive coils (15), are often quite extreme. ARIES-ST for example assumes $\beta_N = 7.4$ with a plasma current of $I_p = 29$ MA in a $R = 3.2$ m, $A = 1.6$ device and STPP has $\beta_N = 8.2$ with $I_p = 31$ MA, $R = 3.4$ m and $A = 1.4$.

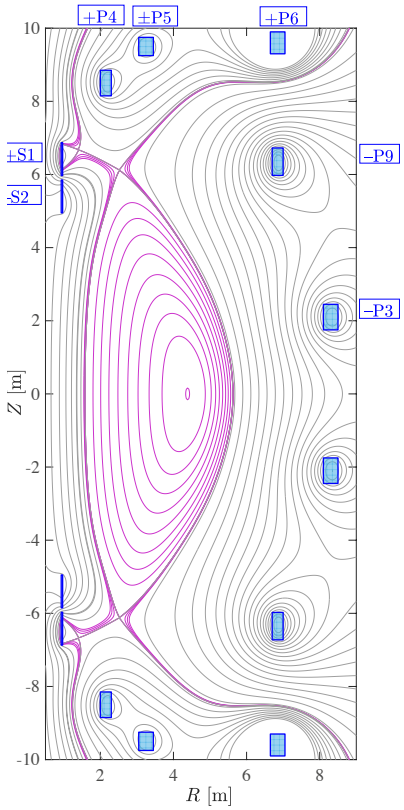

Major Radius	R_{geo} [m]	3.60
Aspect ratio	A	1.8
Toroidal field	B_t (R_{geo})[T]	3.2
Triangularity/Elongation	δ/κ	0.5/3
Plasma current	I_p [MA]	20.5
Fusion power	P_{fus} [GW]	1.53
Net electric power	P_{el} [MW]	67
EC power	P_{EC} [MW]	150
Core radiated power	P_{rad} [MW]	311
Fusion gain	Q	10.2
Normalised β	β_N	4.4
Bootstrap fraction	$f_{BS} = I_{BS}/I_p$	0.88
Greenwald fraction	$f_{GW} = \bar{n}/n_{GW}$	0.95
Internal inductance	l_i (3)	0.28
Effective charge	Z_{eff}	2.7
Minimum safety factor	q_{min}	2.3

Figure 1: Flux contours (pink) of the equilibrium for a high-density electron cyclotron (EC) wave resonance only heated flat top operating point (EC-HD) with a table of respective plasma parameters. The poloidal field shaping coils are shown in blue.

In the following sections we will discuss the basic design philosophy, the major design drivers, the challenges that arise from fully non-inductive operation during the flat-top phase of a pulse, before describing the major gaps in the physics basis and outlining the path to improve confidence in the solutions. Whilst this paper concentrates on the design philosophy many quantitative assessments shown in the paper have been done for specific scenarios which are described in more detail in (1) (22). Most commonly a high density $f_{\mathrm{GW}} = \bar{n}/n_{\mathrm{GW}} \approx 0.95$ ($n_{\mathrm{GW}} = 10^{20}\frac{I_{\mathrm{p}}[\mathrm{MA}]}{\pi a^2}$ m^{-3}: Greenwald density), $I_{\mathrm{p}} = 21$ MA, $P_{\mathrm{HCD}} = P_{\mathrm{EC}} = 150$ MW, $Q = 10$ electron cyclotron (EC) resonance heated only point with a radiated power

fraction in the core of $f_{\mathrm{rad}} = \frac{P_{\mathrm{heat}}}{P_{\mathrm{rad}}} = 70\%$ has been used (EC-HD). Figure 1 shows an equilibrium plot and lists typical parameters for one of the current design point indicating typical parameters.

2. Basic design philosophy

The overall philosophy for STEP plasma scenario design is to facilitate the key benefits of the ST whilst aiming to be as conservative as possible with the assumptions. Nevertheless, at the beginning of the project a wide trade space was explored, and a broad range of scenario families and attributes were assessed for their merits, such as

- Positive versus negative triangularity.
- Different heating and current drive (HCD) schemes and mixes.
- Double null (DN) versus single null (SN) diverted solutions.
- H-mode like edge versus L-mode or I-mode like edge.
- The presence of internal transport barriers

The above characteristics have a somewhat binary character, but most of the performance-defining quantities have a continuous spectrum. For these, optimisation paths were defined, and specific parameter scans were performed to understand the interaction between the different optimisation strategies. The parameters for the viable plasma scenario are also constrained by the choice of HCD system (e.g. B_t and plasma density n_e for RF or microwave based HCD schemes), plasma control and engineering, and cost considerations.

The assessment was done for the flat top operating points (FTOPs) only based initially on a 0D plasma description in a systems code PROCESS (23). For promising designs and to understand interdependencies within the plasma better, the 1D transport solver JETTO (24) was used as detailed in (25) and (22) to map and optimise the parameter space. Since reliable reduced transport models appropriate to STEP-like conditions do not yet exist (see section 4.1). JETTO is used in "assumption integration" mode to build a 1D description of a steady-state non-inductive plasma (zero loop voltage) with self-consistent profiles, transport, heating, current drive and fusion sources, impurities, radiation, and fuelling, with a 2D fixed boundary equilibrium. The boundary shape is iterated to be consistent with free boundary modelling. The β_N is used as an input parameter, and the gyro-Bohm (gB) transport is adjusted until the target is met. The coefficients of the gB model are set with dominant electron transport, as expected for the kinetic ballooning modes (KBMs) and microtearing modes (MTMs) found in STEP conditions (section 4.1). Studies using an extended equilibrium code SCENE coupled with linear gyrokinetic calculations provided guidance for beneficial equilibrium quantities in the core (26). To achieve the required fusion performance, here $P_{\mathrm{fus}} \leq 1.5$ GW for net power production largely determined by the effective thermal cycle efficiency and stationary losses (27) in a compact design, a positive triangularity plasma with a double null primary divertor configuration and a narrow transport barrier at the edge (H-mode like) is the most promising candidate. H-mode (28) is ubiquitous in diverted tokamak devices when the ion heat flux through the separatrix exceeds a certain value, but often exhibits edge localised modes (ELMs) that require special attention for reactor relevant devices. For HCD microwave-based methods that exploit the electron cyclotron resonance such as electron cyclotron heating current drive (ECRH, ECCD) and electron Bernstein wave heating and current drive (EBW, EBCD) give the overall best performance with respect to wall plug efficiency, design integrability and access to all radii (29).

The pressure of the pedestal forming in H-mode is estimated using a scaling $p_{ped} \propto I_p^{0.8} f_{GW}^{0.45}$ derived from the pedestal prediction code EPED (30) for STEP-like conditions. The current drive profiles use simple scaling with a fixed normalised current drive efficiency $\zeta_{\mathrm{CD}} \propto T_e/n_e$ calibrated against more sophisticated modelling (section 3.3) and the heating profile is adjusted to give the desired q profile (section 3.4) using a genetic algorithm (31). The fuelling is assumed to be dominated by pellets with a deposition profile around normalised minor radius $\rho \sim 0.7$. The particle confinement time is assumed to be $\tau_P \sim 4\,\tau_E$, based on integrated modelling of JET discharges (32) and consistent with the experience on conventional aspect ratio tokamaks. Argon is needed for the exhaust solution and a content of 0.5% is assumed. Helium ash production is computed self-consistently with fusion reactions giving ~9% saturated content. Xenon is assumed to be seeded within the pellets and the content is adjusted to give a core radiation power fraction $f_{rad} \approx 70\%$ (larger core radiation fractions are assumed to lead to control problems). The first wall material in SPP will likely be tungsten. For permissible W concentrations in the plasma the radiation from W can likely be compensated by reducing the Xe concentration. Ideally, the core radiation fraction is minimised, but the plasma exhaust requirement of $\frac{P_{\mathrm{sep}}}{R} \sim 40$ MW/m sets an upper limit for the power crossing the separatrix $P_{\mathrm{sep}} = P_{\mathrm{heat}} - P_{\mathrm{rad}}^{\mathrm{core}}$. The JETTO runs are progressed to steady state with a fully relaxed current profile, producing outputs of plasma current, plasma equilibria, kinetic profiles, safety factor (q) profile, current drive (CD) profiles, f_{BS}, fusion power and Q (22). In "assumption integration" mode, confinement is assumed, and auxiliary power and fusion gain are determined by the steady state current drive power requirements. If confinement is predicted not assumed, then fusion gain is extremely sensitive to confinement assumptions (as shown by the simple predictive simulations (1)). For the FTOP only the steady state is considered.

The strong scaling of fusion power with κ and β_N drives the design to a solution with a broad current profile, high elongation and high plasma pressure. The latter is best achieved with high triangularity as the achievable stable pedestal pressure

increases strongly with triangularity (see also section 4.2) and an H-mode like edge. The plasma confinement is generally determined by the plasma current (33), which in a non-inductive burning plasma is determined by the fusion power itself and the auxiliary heating and current drive. The integrated modelling shows that the confinement assumption is strongly related to the auxiliary current drive efficiency. This is another reason why heating systems with high current drive efficiency at high density are very beneficial for fusion power plants (see section 3.3).

The scenarios are routinely checked for fixed boundary ideal MHD stability to n = 1 to 3 modes, and to infinite-n ballooning. As discussed below, the low aspect ratio and choice of q-profile is beneficial in giving strong stability to neoclassical tearing modes. Also as discussed below, and in the companion paper on plasma control, resistive wall modes (RWMs) may be unstable and so RWM control coils are being explored (34).

3. Major Design Drivers

There are various options in designing the flattop operating point that have a major influence such as negative triangularity versus positive triangularity configurations, the plasma exhaust requirements, the heating and current drive requirements, the choice of the q-profile and its implication to plasma stability, the effects due the toroidal field design or the challenges of requiring a largely non-inductive plasma solution. These are briefly discussed in the following sections.

3.1. Negative versus positive triangularity

Plasmas with negative triangularity (NT) were considered as an option for STEP. Such plasmas have been found to have some attractive confinement properties in conventional aspect ratio tokamaks (see for example (35)) and are naturally ELM-free. They are also beneficial for the plasma exhaust as the target area is increased. However, the MHD stability properties of NT plasmas are much worse than those of positive triangularity (PT) plasmas. In the PT case the design relies on access to second ballooning mode stability (see below), but for NT this is not possible (36), and negative triangularity also leads to a greater restriction on the core pressure to avoid strong KBM instability (36). Furthermore, internal low n instabilities are found to dominate over external kink modes (which result in resistive wall modes); this is similar to results found in conventional aspect ratio tokamaks (37). Consequently β_N is optimised by increasing the magnetic shear in the core, with the central safety factor $q(0) \sim 1$, but is still limited to $\beta_N \sim 3$. The lower $q(0)$ leads to higher internal inductance in optimised NT plasmas compared to PT ones, and a limit on the achievable plasma elongation that is ~30% lower. In summary, the key ST advantages of high κ and β_N cannot be realised with NT, and for this reason it was decided that STEP plasmas should have positive triangularity.

3.2. Managing the Exhaust

The burning plasma phase presents a clear exhaust issue for STEP, with a total heating power of $P_{\mathrm{heat}} \approx \frac{P_{\mathrm{fus}}}{5} + P_{\mathrm{HCD}} \sim 500$ MW and considerable He generation, occurring over hours of steady state operation per day. However, unlike conventional reactor designs, such as DEMO, that use a solenoid to drive plasma current, the non-inductive ramp-up phase also presents a significant exhaust challenge in STEP, comparable to the burning phase, due to the need for high auxiliary power injection of the order of $P_{\mathrm{HCD}} \lesssim 200$ MW for external current-drive derived from JETTO calculations (1).

To distribute the heat over a large area impurity seeding is used. Xe is fore seen as main core radiator and Ar is used in the edge and scrape-off-layer. Up to 70% of the loss power is anticipated to be radiated before crossing the separatrix, with the radiation increased above the inherent background continuum radiation (i.e., bremsstrahlung and synchrotron) via injection of Xe-doped pellets, leaving approximately 150 MW of remaining power to be exhausted. This remaining power is transported by particles following open field lines in the scrape-off layer (SOL) plasma surrounding the core plasma towards both an inboard and outboard high heat flux handling component known as the divertor. The area over which the power is spread scales with the divertor strike-point radius, the integral power decay length, and the ratio of the poloidal to the total magnetic field. Therefore, while a higher fraction of power is inherently directed to the outboard divertor, the low inner divertor strike-point radius in STEP, characteristic of a compact ST, results in significantly higher particle flux at the inboard divertor. The design of the divertor can either follow a conventional single null (SN) design, following the foreseen geometry in ITER and DEMO, or an alternative divertor configuration. Alternative divertor configurations typically assessed in current machines (e.g., MAST-U (38)) include a double null (DN) configuration, extended divertor strike-point radii, and the inclusion of an additional X-point near the targets. Figure 2 shows the current design of the divertor in the modelling.

A SN configuration uses a single set of inboard and outboard divertors located either at the bottom or top of the machine, while a double null (DN) configuration uses two sets of inboard and outboard divertors located both at the top and bottom of the machine to increase the area over which the power is spread. Compared to the DN, the SN configuration provides clear benefits: there is easier maintenance access to the machine end opposite to the divertor, there are half the number of components to fail in the divertor, and it reduces the complexity of the vertical position control system as less accuracy is required. However, for perspective, if the SN conventional divertor geometry were scaled into STEP, then the parallel particle flux at the outboard divertor target would be approximately double that expected in DEMO and triple at the inboard

divertor, assuming equivalent upstream plasma conditions. Furthermore, due to the smaller machine size of SPP, there would be major spatial integration challenges with incorporating, around a single divertor, the 24 cryogenic pumps (39). To exhaust the He in the current design an effective pumping speed of $S_{\mathrm{pump}}{\sim}30\ \mathrm{m}^3/s$ is required in the SOLPS-ITER modelling. The study also showed that the requirements during the non-inductive ramp up would lead to a very large device negating the advantage of the ST. Therefore, in summary, the SN configuration was ruled out for STEP and an up-down symmetric DN configuration was adopted. However, maintenance access and accurate vertical position control remain issues with various solutions still under consideration.

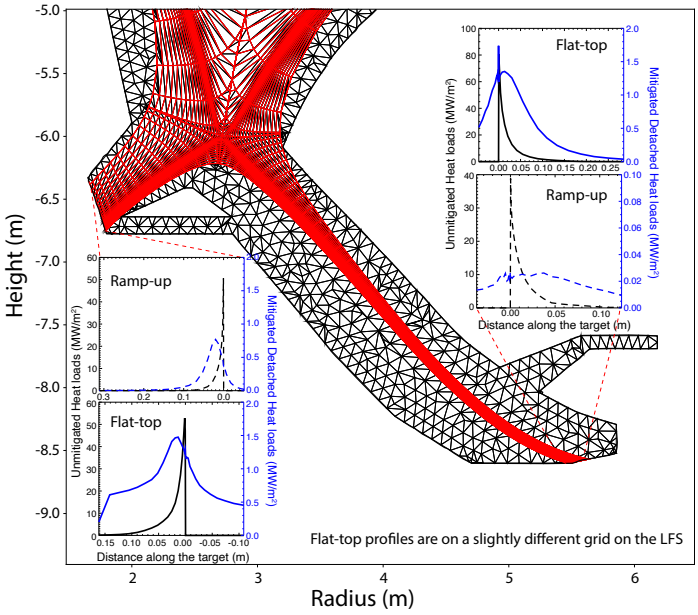

Figure 2: SOLPS-ITER grid and typical unmitigated and mitigated heat load profiles in the flat-top and current-ramp up $I_{\mathrm{p}} = 10$ MA.

Extending the outer divertor strike-point radius, with tight baffling of the divertor region, provides the benefit of widening the detachment window, reducing the demand on the Ar seeding by ~30%, and increasing the level of power transient that can be buffered. An equivalent extension of the inboard divertor radius is not possible, and therefore an additional X-point was introduced near the inner divertor target, but outside of the wall boundary (i.e., approaching an X-divertor). This configuration results in flared flux surfaces at the target, providing a more even distribution of recycled neutrals and thus facilitating detachment across the entire divertor target (40). However, since only the outboard divertors are pumped, the increased number of neutrals recycled into the SOL in this configuration result in higher numbers of impurities (e.g., He) travelling upstream into the core plasma, in comparison to the conventional divertor geometry. An ITER-like dome structure (41), providing a passage between the inner and outer divertors without a direct line-of-sight to the core plasma, has been implemented to maximise the number of recycled particles reaching the outboard pumps.

Despite the advanced divertor design, the concentration of Ar required to dissipate the remaining power directed to the divertors still remains high, ranging between 2 - 4 % throughout the current ramp-up and flat-top, depending on the assumption of radial transport coefficients set as input in SOLPS-ITER simulations (42). It is estimated that the core Ar concentration must be below 0.5% to avoid significant dilution of fuel. Current experiments typically measure a factor two decrease in Ar concentration between the SOL and core (43, 44)]. It is expected that the strong temperature gradient in the plasma edge in STEP will drive an outward neoclassical drift (45, 46), thus screening the core of Ar beyond the values measured in current machines; however, the extent of this screening is so far unknown. Increasing the divertor pressure could be considered to reduce the demand on the Ar puffing (47, 48), however this may not be compatible with the ramp-up phase, which would require low divertor pressure (hence low plasma density). In summary, the chosen divertor design and exhaust plasma solution in STEP presents a potentially viable integrated scenario with sufficient fusion power gain, albeit with notable challenges, such as high Ar concentration, maintenance, and vertical control, that need further investigation.

3.3. Constraints due to the HCD scheme

STEP uses exclusively microwaves for the heating and current drive actuators. This decision resulted from a detailed assessment of current drive efficiency, electrical efficiency, functional suitability, technological readiness, cost, reliability, availability, maintainability and inspectability (29). For the ST, this means either Electron Cyclotron Current Drive (ECCD) or Electron Bernstein Wave Current Drive (EBCD). ECCD is the primary current drive actuator, due to its maturity and flexibility, while EBCD is maintained in the design process, primarily because of predictions that it would deliver a much higher current drive efficiency. It would also allow operation at higher density and thus higher fusion power (49, 50).

The use of ECCD plays an important role in the selection of the magnetic field and density combination in the STEP prototype. It was initially assumed that 2nd harmonic ordinary (O-)mode would be used, requiring as a minimum the 2nd harmonic to be above the O-mode cut-off at the magnetic axis. For EBCD a low-field-side ordinary-extraordinary-Bernstein (O-X-B) mode coupling would be used (51), requiring the fundamental to be lower than the O-mode cut-off. As a design guide, for EBCD access we have used the more stringent condition that the left-hand X-mode cut-off is above the fundamental at the magnetic axis. This has the effect of ensuring that the coupling layer is towards the outer layers of the plasma, which support higher density gradients and where higher coupling efficiency can be expected. Figure 3 shows the region of overlap between these constraints and where the EC-HD FTOP (1, 22) sits. From an ECCD perspective, 2nd harmonic O-mode access to the core is guaranteed by this approach and fundamental O-mode will also be accessible from the high field side of the device.

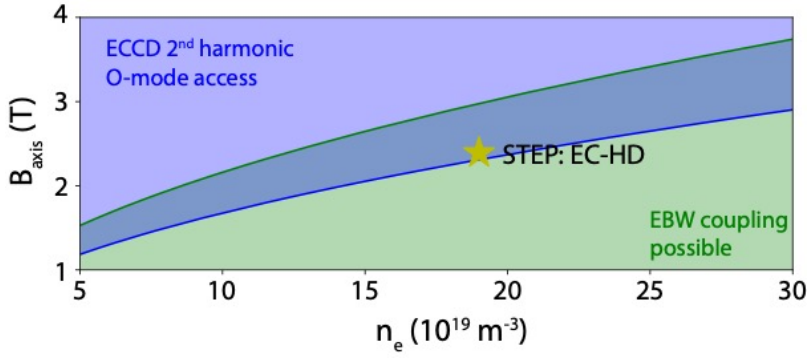

Figure 3. Limitations for ECCD and EBCD access. The blue region indicates the area of parameter space where 2nd harmonic O-mode access is possible, while the green region indicates where low field side EBW coupling can occur. The star indicates where the EC-HD FTOP lies in this parameter space and field and density for this point are calculated at the magnetic axis.

The CD efficiency in units of A/W, η_{CD}, can be usefully normalised to remove variations with radius, temperature, and density (52):

$$\zeta_{\mathrm{CD}} = 3.27 \frac{R_m n_{19}}{T_{keV}} \eta_{\mathrm{CD}}, \tag{2}$$

where R_m is the major radius of the geometric centre of the outermost flux surface in m, n_{19} is local electron density in units of 10^{19} m^{-3} and T_{keV} is local electron temperature in keV. For the EC case, the assumption that ζ_{CD} is approximately constant across the plasma is used to quickly develop an operating point without the need for extensive beam tracing analysis. The validity of the assumption is then checked with extensive scans in frequency, position and launch angle of EC launchers using the GRAY beam tracing code (53). The results of this analysis can then be used to recalibrate ζ_{CD} if necessary, and also find the optimal launch configuration for that scenario, which then also guides the EC engineering design (54). For the EC-HD FTOP it is found that the auxiliary current profile can be matched most efficiently by using a range of frequencies, with 4-5 frequencies being recommended. In addition, at least 1 frequency above 170 GHz is required for the target efficiency. EBCD uses frequencies in the range 90-100 GHz, and relativistic ray tracing shows that it can only be used to access the core at low parallel refractive index (55), which leads to low current drive efficiency. Fokker-Planck simulations using the bounce-averaged, relativistic code CQL3D (56) show the off-axis current drive (at $\rho > \sim 0.6$) for EBCD is dominated by the Ohkawa mechanism on the low-field side of the plasma and exceeds the ECCD efficiency by at least a factor of 2 (50).

Overall the HCD system needs to have sufficient redundancy and margin for both heating schemes (ECCD only and EBCD + ECCD). In a non-inductive burning plasma scenario the fusion power at constant Greenwald fraction has a strong non-linear increase with the HCD power (1). Oversizing the HCD system mitigates the risk of an underperforming plasma. Furthermore, to achieve relevant plasma currents during the no (H) or "low" activation (D) phases that are required for plasma commissioning the missing fusion power and bootstrap current has to be replaced by the HCD system. Therefore, the HCD system is being sized to provide 300 MW of injected power. So far only a few scenarios simulations for the commissioning phase have been done indicating that such power levels should be adequate.

3.4. Choice of safety factor profile

The safety factor profile, q, is chosen to be monotonic with $q_{\mathrm{min}} \geq 2.3$, and maximised shear on rational surfaces. Additional constraints discussed in (27). The choice of q_{min} is consistent with high f_{BS} and with the low internal inductance $0.25 < l_i(3) < 0.3$ needed to allow high κ plasmas. It also avoids the low order resonance at $q = 2$, where potentially disruptive neoclassical tearing modes (NTMs) may occur. Further, elevated q_{min} is consistent with direct access to second ballooning mode stability (57). Studies to optimise the q-profile are yet to be conducted, and it may be the case that higher q_{min} values than those used so far are found to be optimal, as shown in (58). Nevertheless, the q-profiles of the equilibria

used so far provide a good basis for STEP FTOPs: they are stable to internal MHD instabilities and NTMs with $n = 1$ and 2. Modelling of NTMs, validated against experimental results from several devices including the MAST ST (59), shows strong curvature stabilisation at low aspect ratio (60), which suppresses the excitation of NTMs with $m = 3$, $n = 1$ and $m = 5$, $n = 2$. Since the equilibria tend to have low shear in the core, it is found that $q_{\min}$ above about 2.2 is necessary to prevent infernal mode (61) from being either unstable or close to instability and coupling to RWMs.

3.5. Constraints for the toroidal field design

It is envisaged at present that STEP will have picture-frame toroidal field (TF) coils with vertical outer limbs (62). In such cases the toroidal ripple in the equilibrium magnetic field arising from the use of a finite number of coils N is a function of major radius only inside the plasma, and the perturbations to the field components in right-handed cylindrical coordinates (R, φ, Z) can be well-approximated by the expressions (63)

$$\tilde{B}_R = \frac{B_0 R_0}{R}\left(\frac{R}{R_{coil}}\right)^N \sin N\varphi, \qquad \tilde{B}_\varphi = \frac{B_0 R_0}{R}\left(\frac{R}{R_{coil}}\right)^N \cos N\varphi, \qquad \tilde{B}_Z = 0, \tag{3}$$

where R_{coil} is the outer limb coil radius and B_0 is the field at the magnetic axis, $R = R_0$. Any such perturbations violate conservation of toroidal canonical momentum, and thereby degrade fusion α-particle confinement. Any non-axisymmetric ferromagnetic structures in the tokamak assembly will also modify the magnetic field but are not considered here.

The choice of N is determined largely by engineering constraints, in particular ease of maintenance and port access: the baseline value of this parameter is 16. It is typically assumed that fast ion losses are likely to be acceptable if the ripple amplitude $\delta = \tilde{B}/B_0$ does not exceed a value of around 1% anywhere in the plasma. For the field perturbation given by equation (3) the maximum occurs at the outer midplane plasma edge where, in currently used STEP FTOPs, $R \simeq 5.6$m. It can be inferred from equation (3) that a minimum coil radius satisfying this condition is about 7.5m. This is a useful first estimate, but a reliably safe value of R_{coil} can only be calculated by simulating α-particles for about a collisional slowing-down time from birth in a realistic equilibrium field with the ripple perturbation superimposed, and using a model for the first wall so that precise loss criteria can be defined, and α-particle power loading maps can be generated. For this purpose we have used the GPU-based LOCUST code, which can track a sufficiently large number of markers that accurate estimates of the maximum power loading can be obtained (64). Figure 4 shows the maximum α-particle power loading versus R_{coil} for $N = 16$. This illustrates the high sensitivity of the ripple-induced losses to the perturbation amplitude and confirms that R_{coil} for this number of coils should be around 7.5m or more: the peak loading in this case occurs on the tungsten armour on the low field side of the main chamber wall where the maximum tolerable load due to all non-neutronic sources (thermal plasma, high energy α-particles and electromagnetic radiation) is around 1-2 MWm^{-2}.

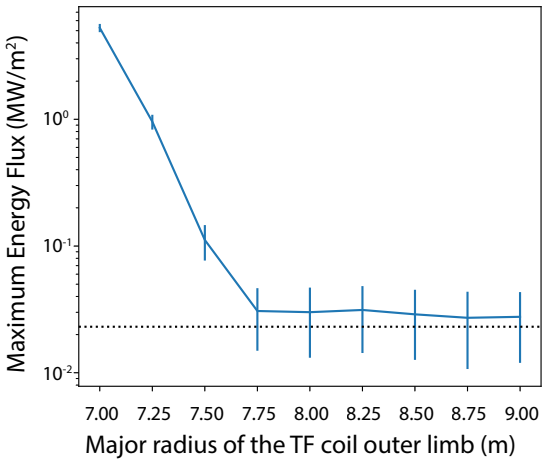

Figure 4: Maximum power loading on the first wall due to prompt and TF ripple-induced α-particle losses versus TF coil outer radius for the case of 16 coils.

These results depend on the exact values of B_0 and I_p (respectively 2.5T and 20.5MA for the FTOP used here), since these determine the α-particle orbit width. It should be noted that α-particles can also in principle be lost due to both self-driven instabilities (toroidal Alfvén eigenmodes (65), for example) and unstable modes of the bulk plasma (such as NTMs and RWMs). Analysis so far indicates that TAEs in STEP will be strongly-Landau damped by bulk ions, while the impact of controlled RWMs on α-particle confinement is likely to be negligible (65). The effects of other instabilities will be considered in future work.

3.6. Challenges for the non-inductive scenario

The space in the centre of an ST power plant is very precious and implementing a solenoid that allows the generation of the full plasma current is impossible with the current technologies. Whilst a design without a solenoid would be preferable

a small solenoid can mitigate the considerable risk of not being able to form a plasma. Non solenoidal start-up schemes have been studied for STs (66) experimentally and is a very active field of research, but the theoretical framework to allow extrapolation to STEP is missing. A small solenoid, $\Delta\psi_{CS}{\sim}9\,Vs$, is foreseen as a proven start-up technique that can be accurately modelled with the DYON code (67) and for the inductive ramp up to a low current full bore diverted target plasma for the non-inductive ramp-up (68, 69).

A key challenge for the non-inductive current ramp-up is the avoidance of a current hole on axis. As the resistivity is a strong function of T_e it is likely to have a broader heat and current deposition profile than the conductivity profile. The auxiliary current drive will cause an electric field that tries to counter the current drive (back-EMF) due to Faraday's law. This will drive a counter current in the plasma with a different profile to the driven current leading to a current hole. To avoid this current hole due to the interaction between Faraday's law and the slow current diffusion in a hot plasma the increase in the plasma current by increasing the auxiliary power has to be done gradually from the centre on the current diffusion time scale. This can be achieved by growing the plasma boundary with a fixed $j(\psi)$ or by broadening the profile using the flexibility of the heating and current drive (HCD) system (68). The latter is more advantageous with respect to divertor performance and vertical stability (34). The overall power of the HCD system needs to be kept as low as possible to keep the heat exhaust in the divertor manageable. The current drive efficiency $\eta_{CD} \propto T_e/n_e$ favouring on the one hand a hot low-density plasma. On the other hand, the divertor constraint requires a certain minimum density and also the fusion power increases like $P_{fus} \propto n^2$ favouring a high density FTOP. These contradicting requirements have to be balanced during the ramp-up whilst additionally maintaining MHD stable current profiles. To achieve net electricity $P_{fus} \gg P_{HCD}$ and the overall current must be dominated by the pressure driven bootstrap current (70). At fixed heating power the interplay between density, current drive efficiency and bootstrap current leads to a minimum of I_p as function of density (22), that must be overcome to reach the final high density FTOP. This leads to a ramp-up scenario where first the full current is generated on a long-time scale $O(h)$ at the lowest possible density and then at full current the plasma density is increased within 10s – 100s to reach the fusion conditions (68). In small devices with high electron heating a clamping of the ion temperature has been observed (71) that poses a certain risk to the ramp-up scenario depending on the underlying turbulence. At full current for STEP the beneficial ratio of energy exchange time to confinement time should allow to reach $T_i{\sim}T_e \approx 20$ keV needed for efficient fusion. To avoid the current hole in the flat-top phase a small amount of central HCD is also required. The current ramp down faces different issues, namely the avoidance of the radiative collapse and maintaining a low l_i. To speed-up the ramp-down and to reduce the stored energy in the plasma it is advantageous to maintain a high density and to reduce the fusion power at high plasma density by changing the fuel from DT to D. In addition, the transition from H-mode back to L-mode needs to be delayed as long as possible to have the corresponding β and l_i change at the lowest possible current.

The toroidal magnetic field on-axis is set by the electron cyclotron resonance conditions, and thus the minimum ST device size is set by the engineering design of the centre post. Integrated modelling studies for this minimum device size show that, to attain adequate fusion power ($\sim \beta_N^4$ at fixed f_{BS}), β_N generally needs to be above the no-wall limit for the $n = 1$ external kink mode. Operation in the domain between the no-wall ($\beta_N^{no-wall}$) and with-wall ($\beta_N^{with-wall}$) $n = 1$ kink mode limits means that the RWM is potentially unstable. The exploration of RWM stability for some possible STEP scenarios is discussed in Ref (72). RWM stability is parameterised by a quantity C_β defined as

$$C_\beta = \frac{\beta_N - \beta_N^{no-wall}}{\beta_N^{with-wall} - \beta_N^{no-wall}}.$$

For $0 < C_\beta < 1$ the RWM is potentially unstable while for $C_\beta > 1$ it is ideally unstable (and thus uncontrollable). In the former case stability can be affected by the presence of toroidal rotation. In the fluid limit rotation stabilisation primarily occurs due to ion sound wave damping and coupling to the Alfvén continuum. At low C_β values toroidal fluid rotation can completely stabilise the $n = 1$ RWM, but at values above about 0.5 the fluid rotation becomes ineffective in stabilising this mode (72). Moreover, since STEP has no external momentum input from the proposed microwave-based schemes, bulk plasma rotation will be low and likely to correspond to Alfvénic Mach numbers that are below the values (typically a few percent) needed to attain stabilisation at low C_β. The effect of kinetic resonances on stabilising the $n = 1$ RWM has also been examined. Due to the low plasma rotation, the dominant kinetic resonance is found to be with the precessional drift of the thermal ions (72). The strength of this resonance damping on the RWM depends on the intrinsic plasma rotation, which is poorly known. Also, at higher C_β the effect of the resonance becomes weak, an example of which is shown in Figure 5.

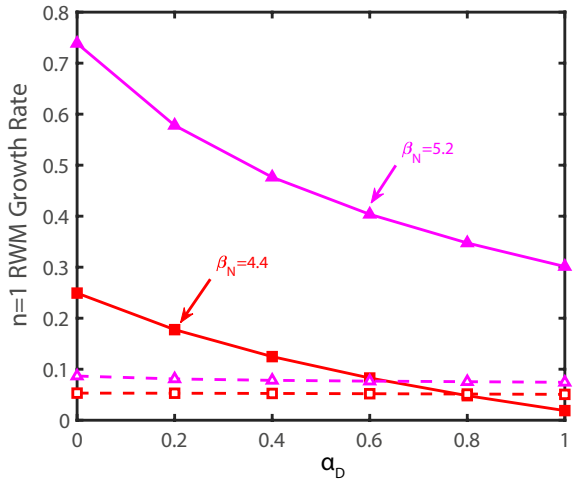

Figure 5: n=1 RWM growth rate (normalised using the wall resistive diffusion time) versus a parameter α_D that controls the degree to which kinetic terms are applied: $\alpha_D = 0$ is the fluid limit and $\alpha_D = 1$ is the fully kinetic limit. The red and pink curves are, respectively, for equilibria with $C_\beta = 0.14$ and $C_\beta = 0.6$.

Given the uncertainties of intrinsic stabilisation of the RWM by toroidal rotation or kinetic effects, STEP is designed to have active RWM control. For some candidate STEP FTOPs it is found that the $n = 2$ RWM can also be weakly unstable. For this reason, the RWM control system is being designed to stabilise both $n = 1$ and $n = 2$ RWMs. The topic of active RWM control in STEP is discussed in the 'Controlling a new Plasma Regime' paper, which is part of this journal issue (34).

4. Major gaps

4.1. Plasma transport

In combination with the available sources of heat and particles, turbulent transport will determine the equilibrium profile evolution and will be a key driver in dictating the fusion power that can be achieved in STEP. Reduced physics-based models of core transport are essential for integrated scenario modelling, and these are very highly developed for electrostatic turbulence, where extensive gyrokinetic simulations and experimental data are available to guide model development and validation. For example, the construction of TGLF (trapped-gyro-Landau-fluid), one of the most advanced physics-based reduced models of core transport available (73), was closely guided by high fidelity local gyrokinetic simulations of electrostatic turbulence. STEP is a high β spherical tokamak: for this reason, the turbulence in its core is expected to be strongly electromagnetic, and thus very different in character from the electrostatic turbulence that dominates in the lower β regime of conventional tokamaks and has been extensively explored in these devices. Limited studies of electromagnetic (EM) turbulence using local gyrokinetics have been carried out. These include simulations of EM turbulence in large aspect ratio model equilibria (74), and of MTM turbulence in the cores of the NSTX (75) and MAST (76, 77). STs, and at the edge of ASDEX-Upgrade (78). However, large remaining uncertainties in the transport associated with electromagnetic core turbulence in STEP mean that plasma confinement is one of the biggest risks to the project.

The transport database for spherical tokamaks is dominated by MAST and NSTX, which have produced plasmas that are useful for confinement studies (13), albeit in non-burning plasma conditions very different from those in the STEP flat-top. In contrast to STEP, neutral beam injection (NBI) typically dominates the heating In MAST and NSTX, giving higher ion heating fractions and stronger toroidal rotation, and the plasmas are at lower β and higher collisionality, ν_*. A strong inverse scaling of energy confinement time with ν_* (stronger than that found at conventional aspect ratio) has been reported independently from NSTX (12) and MAST (11): this is favourable for performance in an FPP based on the ST, provided of course that the scaling extrapolates In (12) it is noted that improving confinement at lower $\nu_\star$ in NSTX was largely achieved through a reduction in electron heat transport, and that in this regime hybrid TEM/KBMs become unstable in the outer plasma where ion thermal transport starts to exceed the neoclassical level.

The highest fidelity model for core turbulence in tokamaks is local gyrokinetics, and this has been exploited, initially neglecting fusion α-particles, to advance our understanding of EM core turbulence in the EC-HD concept design (79, 80). Linear local gyrokinetic simulations close to mid-radius in reveal microinstabilities arising at ion scales in the binormal (orthogonal to both the equilibrium magnetic field and flux surface) wavenumber, with dominant hybrid-KBMs and sub-dominantly unstable MTMs (79). Neglecting equilibrium flow shear, nonlinear local simulations find that the hybrid-KBM turbulence robustly runs away to large heat and particle fluxes that exceed the available sources by orders of magnitude, with heat transport that is dominated by magnetic flutter in the electron channel at the lowest binormal wavenumbers (77). In the runaway state the radial correlation lengths of turbulent structures are in fact too large to be well captured by the local equilibrium model. With sufficient perpendicular equilibrium flow shear, transport and turbulence radial correlation

lengths are significantly reduced. It should be noted, however, that flow shear is expected to be modest in STEP as there is no momentum source from NBI. Nevertheless, including even a diamagnetic level of flow shear lowers the heat flux closer to the total heat source. We caution that diamagnetic flows strictly require higher order theory in $\rho_\star$ to be included self-consistently. (80) also reports that locally increasing the normalised pressure gradient (β') reduces the turbulence to a regime where the associated heat transport reaches a better balance with the sources. This is likely to be related to stabilising impacts of more favourable trapped electron precessional drifts (81), and/or to improved stability to ideal $n \longrightarrow \infty$ ballooning modes (77). As this stabilising effect is reduced at lower pressure gradient, the corollary is that the turbulent fluxes reduce only weakly as the pressure gradient falls, which could make it challenging to gain access to a burning plasma state if this transport cannot be mitigated.

4.2. Operating without Edge Localised Modes (ELMs)

The intermittent instabilities in the plasma edge called ELMs (82) deposit heat on the divertor and can cause significant damage to the plasma-facing components. In STEP, projections based on scalings from current devices indicate that the heat loads from large ELMs would stay below the melting limit of tungsten but could lead to cracking and erosion of the divertor plates. It is intended that STEP will operate in a regime that has either no ELMs or ELMs that are small enough that damage to the divertor is avoided. Such potential operating regimes include quiescent H-mode (QHM) (83-85), quasi-continuous exhaust (QCE) (86-88) and radiative X-point (89, 90). While these regimes have been observed in current conventional aspect ratio tokamaks, a theoretical understanding of why the ELMs are avoided and how much the confinement is degraded compared to ELMy plasmas is still lacking. Furthermore, their applicability to a spherical tokamak in double null configuration has not been demonstrated. Nevertheless, the use of Li for wall conditioning led to an ELM free regime in NSTX (91, 92) and recently an ELM free regime has been observed on MAST-U (93). Modelling to gain an understanding of these regimes and the ability to extrapolate them to STEP is needed, and in particular non-linear MHD modelling of experimental no/small ELM regimes in a spherical tokamak as is done for conventional a tokamak for QCE (94) or for QHM (95) is required. On the experimental side, the MAST Upgrade tokamak offers a testbed to demonstrate their applicability to STs.

In addition to intrinsically no/small ELM regimes, STEP is being designed to have two sets of coils above and below the midplane that will produce resonant magnetic perturbations (RMP) to suppress the ELMs. This method has been demonstrated in numerous tokamaks and is planned to be used in ITER. In STEP it is intended as a back-up system in case the no/small ELM operating regimes fail to deliver sufficient ELM suppression. They may also be used under transient conditions such as ramp-up and ramp-down to ensure ELM-free operation. RMP modelling using a necessary condition for the amplitude of the perturbation that has been found in current devices project that a relatively modest current (compared to the system used in ITER) is required in STEP to reach the ELM mitigation conditions (96). However, it must be noted that full ELM suppression has not been demonstrated either in spherical tokamaks or in double null configuration (the selected plasma configuration for STEP), which makes the above prediction very uncertain. The calculated optimal phase difference for ELM suppression between the currents in upper and lower coils is also not optimal in terms of fusion α-particle confinement (65).

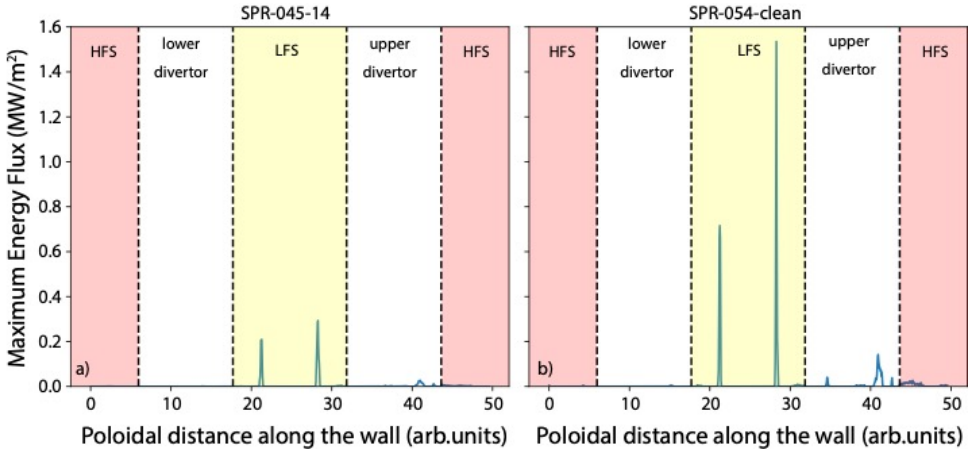

Figure 6 Poloidal distribution of maximum power loading due to prompt and TF ripple induced α-particle losses when $N_{\mathrm{coil}} = 16$ and $R_{\mathrm{coil}} = 7.4$ m for a) the EC-HD FTOP and b) a lower density EC FTOP with a hotter pedestal.

Losses of fusion α-particles need to be considered in pedestal modelling. The stiffness of energy transport typically found in tokamak plasmas means that high temperature and density pedestals are highly desirable in terms of optimising fusion power, but they can also lead to significant α-particle production at the pedestal top. Figure 6 shows the poloidal distribution of power loading due to axisymmetric and TF ripple-induced α-particle losses, again calculated using LOCUST, in two candidate STEP equilibria with slightly different pedestal parameters. The top plots show results for the EC-HD FTOP

while the bottom ones were generated for a lower density variant of this operating point with a hotter pedestal. The fusion power was similar in these two cases. In the top plots the pedestal top ion temperature is 4.4 keV, while in the bottom plots it is nearly 7 keV. Switching to a hotter pedestal results in the peak α-particle wall loading increasing by a factor of more than 5 to around 1.6 MW/m^2, despite a slight reduction in the density, while the total loss of α-particle power rises from 1.1 MW to 2.7 MW (the latter is about 0.8% of the α-particle power). It can be seen in Figure 6 that the highest power loading occurs on the low field side of the main chamber, where the maximum tolerable heat flux is around 0.7 MW/m^2. Moreover, higher losses and power loadings occur when three-dimensional field perturbations are present, including the TF ripple discussed above, but also those due to ELM control coils, error fields, instabilities, and non-axisymmetric ferromagnetic materials. It should be noted that whilst increasing the pedestal pressure is very beneficial for the fusion performance the α-particle losses will set a limit to this optimisation depending on the actual 3D perturbations as well as the plasma wall gap.

4.3. Runaway Electron mitigation

Since STEP flat-top operating point has a large plasma current I_p(~20MA), any plasma disruption is likely to induce large electromagnetic forces in conducting structures as well as a high current runaway electron (RE) beam. This is mainly due to the large plasma current, as the avalanche rate of REs scales exponentially with I_p (97). As in the cases of ITER (98) and SPARC (99), STEP thus falls into the seed-insensitive regime of RE generation, meaning that even small RE seeds, including those from sources that are almost impossible to mitigate (for example tritium decay or Compton scattering), can quickly avalanche during disruption current quenches (CQs). This has been confirmed by modelling unmitigated disruptions in STEP with the code DREAM (100), using various assumptions for the thermal quench (TQ). To mitigate this, STEP concept design includes an extensive set of shattered pellet injectors (SPIs) that follow requirements set by DREAM simulations of SPI-mitigated disruptions (101). This strategy is largely in-line with ITER. One difference with ITER is that high-field side (HFS) pure D_2 pellet lines are planned to make use of so-called plasmoid drifts (102) and reduce the generation of RE seeds pre-CQ (through the hot-tail mechanism). The efficacy of this strategy has been shown for previous STEP concepts (103), but it can't avoid the generation of a large current RE beam (> 12 MA) when using the latest version of the EC-HD FTOP and the DREAM SPI model (101): see Figure 7.

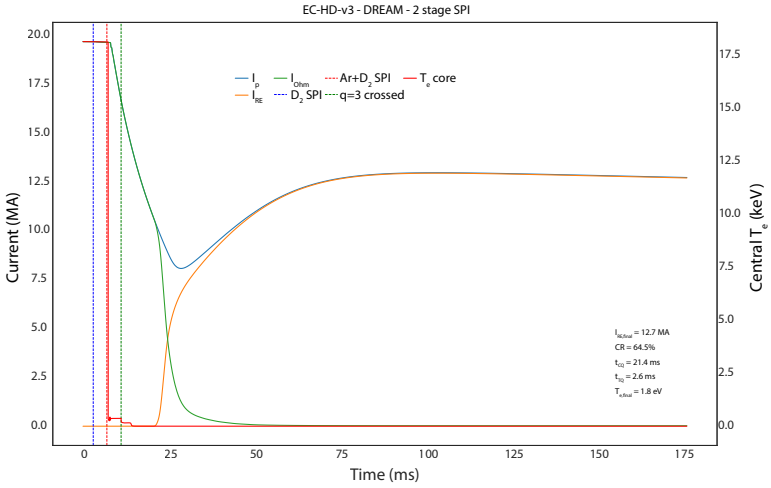

Figure 7: Results from DREAM simulations of a STEP-mitigated disruption, with injection of 2-stage shattered pellets (pure D_2 at 3ms, then Ar + D_2 at 7ms). The runaway electron beam is mitigated compared to the no-injection case but remains very high, at 12.6 MA for a 1ms TQ with $\delta B/B = 0.2\%$.

Consequently, STEP concept design also includes multiple pure D_2 SPI lines dedicated to RE beam mitigation. Those lines will be used to change the properties of the background plasma during the RE plateau phase, to achieve a benign termination of such a RE beam (104, 105). This method has been successfully applied in several current devices (TCV, ASDEX-Upgrade, DIII-D), including JET (106), and will also be used on ITER. However, due to the remaining uncertainties and possible limitations of this method (arising from re-avalanching, upper limit for D_2 injection), the STEP team is now investigating complementary methods to achieve RE beam mitigation. One of those is to use a passive runaway electron mitigation coil (REMC) to induce magnetic field perturbations during the CQ that are large enough to counteract the avalanche. This strategy has been successfully modelled for SPARC and DIII-D (99, 107, 108) and will be tested in those devices in the next few years.

4.4. Key Research Needs

The most urgent single plasma priority in terms of plugging the gap between present-day STs and STEP is the development of a first principles-based understanding of core confinement in the high beta regime needed to achieve burning plasma

conditions. High priorities for future work in this area, some of which is already in progress, include: (i) building a reduced model to describe transport fluxes from hybrid-KBM turbulence, and exploring the use of machine learning (ML) surrogates to accelerate the evaluation of such models (see e.g. (109)); (ii) performing flux-driven simulations using such physics-based models to predict profiles for the STEP FTOPs; (iii) performing the first global gyrokinetic simulations of hybrid-KBM turbulence (which will require the inclusion of compressional magnetic perturbations, $\delta B_{\parallel}$, usually omitted in global gyrokinetics); (iv) assessing the impacts of fusion α-particles and other impurities on microturbulence; (v) improving our understanding of the onset of runaway heat fluxes; (vi) seeking accessible experimental regimes in both current and planned devices where validation may be possible; and (vii) studying turbulent transport and the validity of reduced models in the STEP ramp-up. These studies must include the aspects of momentum transport as the turbulence has been found to be very sensitive to plasma rotation. The strong flow shear dependence of the hybrid-KBM mode poses a challenge as present day STs assess high β with substantial torque input. In addition, an understanding of impurity transport in the STEP relevant regimes (high β, high $q_{\min} > 2.3$, slow rotation) needs to be established including the transport through the pedestal. This is important in-particular for W transport. It should be noted that no ST with a high-Z metal wall exists.

Research on no/small ELM regimes in high performance, double null STs is also key for the development of viable FTOPs for STEP. This will be among the primary future goals of MAST-U and NSTX-U. The former device will also provide a vital opportunity to validate modelling of EBCD in an ST, since it will be equipped with two gyrotrons delivering nearly a megawatt each of microwave power from around 2025 onwards. Accessing high beta regimes in MAST-U and NSTX-U is expected to provide essential data not only on core transport under STEP-like conditions, as noted above, but also on α-particle physics: it is predicted that many of the instabilities driven by energetic ions in present-day devices will be suppressed In STEP, either because of thermal ion Landau damping or the absence of significant fast ion anisotropy (65), but again experimental validation of these predictions is lacking. Finally, MAST Upgrade has been specifically designed to test advanced divertor concepts, and for the development of STEP-relevant scenarios that combine high core plasma performance and radiation with detached exhaust plasma operation. It is clear therefore that MAST Upgrade will play a key role in the STEP project.

5. Conclusions

The following conclusions have emerged from the UKAEA programme to design a first-of-a-kind fusion reactor delivering net electricity, based on the ST concept: (i) a double null configuration is likely to be needed to ensure that exhaust power loads are manageable on the commercial reactor scale; (ii) microwaves (rather than neutral beams or radio-frequency waves) provide the most effective actuator for external heating and current drive; (iii) plasma cross-sections shapes with positive triangularity are far preferable to those with negative triangularity, due to unfavourable limits on the normalised plasma pressure (and hence fusion performance) in the latter case; (iv) equilibria with safety factor $q > 2$ across the entire plasma have robust stability properties; (v) the indications so far are that the presence of fusion α-particles needn't lead to any difficulties in terms of either unacceptable power loads on plasma-facing components or kinetic instabilities; (vi) a complex mitigation scheme will need to be in place to manage the risk of a plasma disruption, even if the control system ensures that such events are extremely rare; (vii) the turbulence regime in the core plasma will be qualitatively different from that in any existing device, and pushes presently-available simulation codes to their limit, both in terms of computing resources and physics models; (viii) there are large uncertainties in how to achieve conditions such that confinement is good enough to generate net electricity and in which ELMs are either non-existent or present but manageable. These last two conclusions mean that STEP remains a high-risk project (there are of course other, non-plasma risks, discussed in other papers of this special issue).

We comment finally that several of these conclusions are specific to ST-based reactor concepts, and indeed in some cases underline inherent advantages of the ST concept. On the other hand, there is a lot of synergy between the STEP work and the solutions needed for power plants based on the conventional aspect ratio tokamak or stellarator concept allowing for a mutual gain. For example, microwave-based external heating and current drive may also turn out to be the best long-term option for power plants. In addition, the need for high plasma current in any tokamak-based reactor means, whilst STEP benefits greatly from the work done in support of ITER, novel disruption mitigation schemes of the type being investigated for STEP may also be attractive for future devices.

Acknowledgments

This work has been funded by STEP, a UKAEA programme to design and build a prototype fusion energy plant and a path to commercial fusion. To obtain further information on the data and models underlying this paper please contact PublicationsManager@ukaea.uk. This work was the effort of a large group of people at UKAEA and invaluable collaborations. For invaluable help in performing the RE studies, the authors would like to thank the Chalmers Plasma Theory group and the MIT group, in particular M. Hoppe (now at KTH), O. Vallhagen and A. Tinguely.

References

1. Meyer H. THE PLASMA SCENARIOS FOR THE SPHERICAL TOKAMAK FOR ENERGY PRODUCTION (STEP) AND

THEIR TECHNICAL IMPLICATIONS. 29th IAEA Fusion Energy Conference; 16-21 Oc.; London, UK2023.
2. Waldon C. Concept Design Overview - A Question of Choices and Compromise. Philosophicsl Transactions A 2024.
3. Kikuchi M, et.al. Fusion Physics: IAEA; 2012.
4. Sykes A, the ST, the NBIT, the MT, the Theory T. The spherical tokamak programme at Culham. Nuclear Fusion. 1999;39(9Y):1271-.
5. Gerhardt SP, Gates DA, Kaye SM, Maingi R, Menard JE, Sabbagh SA, et al. Recent progress towards an advanced spherical torus operating point in NSTX. Nuclear Fusion. 2011;51(7):073031.
6. Menard JE, Brown T, El-Guebaly L, Boyer M, Canik J, Colling B, et al. Fusion nuclear science facilities and pilot plants based on the spherical tokamak. Nuclear Fusion. 2016;56(10):106023-.
7. Valovič M, Meyer H, Akers R, Brickley C, Conway NJ, Cunningham G, et al. Energy and particle confinement in MAST. Nuclear Fusion. 2005;45(8):942.
8. Kaye SM, Bell MG, Bell RE, Fredrickson ED, LeBlanc BP, Lee KC, et al. Energy confinement scaling in the low aspect ratio National Spherical Torus Experiment (NSTX). Nucl Fusion. 2006;46(10):848-57.
9. Buxton PF, Connor JW, Costley AE, Gryaznevich MP, McNamara S. On the energy confinement time in spherical tokamaks: Implications for the design of pilot plants and fusion reactors. Plasma Physics and Controlled Fusion. 2019;61(3):35006-.
10. Kurskiev GS, Gusev VK, Sakharov NV, Petrov YV, Bakharev NN, Balachenkov IM, et al. Energy confinement in the spherical tokamak Globus-M2 with a toroidal magnetic field reaching 0.8 T. Nuclear Fusion. 2021;62(1):016011.
11. Valovič M, Akers R, de Bock M, McCone J, Garzotti L, Michael C, et al. Collisionality and safety factor scalings of H-mode energy transport in the MAST spherical tokamak. Nuclear Fusion. 2011;51(7):73045-.
12. Kaye SM, Gerhardt S, Guttenfelder W, Maingi R, Bell RE, Diallo A, et al. The dependence of H-mode energy confinement and transport on collisionality in NSTX. Nuclear Fusion. 2013;53(6):063005.
13. Kaye SM, Connor JW, Roach CM. Thermal confinement and transport in spherical tokamaks: a review. Plasma Physics and Controlled Fusion. 2021;63(12):123001.
14. Akers RJ, Bond A, Buttery RJ, Carolan PG, Counsell GF, Cunningham G, et al. Steady state operation of spherical tokamaks. Nuclear Fusion. 2000;40(6):1223.
15. Voss GM, Allfrey S, Bond A, Huang Q, Knight PJ, Riccardo V, et al. A conceptual design of a spherical tokamak power plant. Fusion Engineering and Design. 2000;51-52(0):309-18.
16. Wilson HR, Ahn JW, Akers RJ, Applegate D, Cairns RA, Christiansen JP, et al. Integrated plasma physics modelling for the Culham steady state spherical tokamak fusion power plant. Nucl Fusion. 2004;44:917-29.
17. Menard JE, Bromberg L, Brown T, Burgess T, Dix D, El-Guebaly L, et al. Prospects for pilot plants based on the tokamak, spherical tokamak and stellarator. Nuclear Fusion. 2011;51(10):103014-.
18. Najmabadi F. Spherical torus concept as power plants—the ARIES-ST study. Fusion Engineering and Design. 2003;65(2):143-64.
19. Nishio S, others, editors. Technological and environmental prospects of low aspect ratio tokamak reactor VECTOR2004: IAEA.
20. Gi K, Ono Y, Nakamura M, Someya Y, Utoh H, Tobita K, et al. Conceptual design study of the moderate size superconducting spherical tokamak power plant. Nuclear Fusion. 2015;55(6):063036.
21. Costley AE. Towards a compact spherical tokamak fusion pilot plant. Philosophical Transactions of the Royal Society A: Mathematical, Physical and Engineering Sciences. 2019;377(2141):20170439.
22. Tholerus E. Flat-top plasma operational space of the STEP power plant. 2024.
23. Muldrew SI, Lux H, Cunningham G, Hender TC, Kahn S, Knight PJ, et al. "PROCESS": Systems studies of spherical tokamaks. Fusion Engineering and Design. 2020;154:111530.
24. Romanelli M, Corrigan G, Parail V, Wiesen S, Ambrosino R, Da Silva Aresta Belo P, et al. JINTRAC: A System of Codes for Integrated Simulation of Tokamak Scenarios. Plasma and Fusion Research. 2014;9:3403023-.
25. Meyer H. 2.A3: Identify a preferred flat-top plasma scenario for the STEP prototype reactor, coherent with the preferred machine Concept Design, including a plan for the associated risk reduction research required before the end of tranche. Corporate Milestone Report. Internal Report: United Kingdom Atomic Energy Authority, STEP; 2022. Contract No.: CD-STEP-10006.
26. Patel BS, Dickinson D, Roach CM, Wilson HR. Linear gyrokinetic stability of a high β non-inductive spherical tokamak. Nuclear Fusion. 2022;62(1):016009.
27. Acres J. Producing net power. Philosophicsl Transactions A 2024.
28. Team A. The {H}-Mode of {ASDEX}. Nucl~Fusion. 1989;29(11):1959-2040.
29. Henderson M. THE CONCEPT DESIGN OF THE STEP HEATING AND CURRENT DRIVE SYSTEM. 29th IAEA Fusion Energy Conference; 16-21 Oct.; London, UK2023.
30. Snyder PB, Groebner RJ, Hughes JW, Osborne TH, Beurskens M, Leonard AW, et al. A first-principles predictive model of the pedestal height and width: development, testing and ITER optimization with the EPED model. Nuclear Fusion. 2011;51(10):103016.
31. Marsden S, Casson F, Freethy S, Wilson T, Patel BS, Tholerus E. Using Genetic Algorithms to Optimise Current Drive in STEP. 48th EPS Conference on Plasma Physics2022.
32. Casson FJ, Patten H, Bourdelle C, Breton S, Citrin J, Koechl F, et al. Predictive multi-channel flux-driven modelling to optimise ICRH tungsten control and fusion performance in JET. Nuclear Fusion. 2020;60(6):066029.
33. Hazeltine RD, D MJ. Plasma Confinement. New York: Addison-Wesley Publishers; 1992.
34. Lennholm M. Controlling a New Plasma Regime. Philosophicsl Transactions A 2024.
35. Fontana M, Porte L, Coda S, Sauter O, The TCVT. The effect of triangularity on fluctuations in a tokamak plasma. Nuclear Fusion. 2018;58(2):024002.
36. Davies R, Dickinson D, Wilson H. Kinetic ballooning modes as a constraint on plasma triangularity in commercial spherical tokamaks. Plasma Physics and Controlled Fusion. 2022;64(10):105001.
37. Medvedev SY, Kikuchi M, Villard L, Takizuka T, Diamond P, Zushi H, et al. The negative triangularity tokamak: stability limits and prospects as a fusion energy system. Nuclear Fusion. 2015;55(6):063013.
38. Morris W, Harrison JR, Kirk A, Lipschultz B, Militello F, Moulton D, et al. MAST Upgrade Divertor Facility: A Test Bed

for Novel Divertor Solutions. IEEE Transactions on Plasma Science. 2018;46(5):1217-26.
39. Lord M. Fusing Together a Design for Sustained Fuelling and Tritium Self-Sufficiency. Philosophicsl Transactions A 2024.
40. Hudoba A, Newton S, Voss G, Cunningham G, Henderson S. Divertor optimisation and power handling in spherical tokamak reactors. Nuclear Materials and Energy. 2023;35:101410.
41. Pitts RA, Carpentier S, Escourbiac F, Hirai T, Komarov V, Kukushkin AS, et al. Physics basis and design of the ITER plasma-facing components. Journal of Nuclear Materials. 2011;415(1, Supplement):S957-S64.
42. Osawa RT, Moulton D, Newton SL, Henderson SS, Lipschultz B, Hudoba A. SOLPS-ITER analysis of a proposed STEP double null geometry: impact of the degree of disconnection on power-sharing. Nuclear Fusion. 2023;63(7):076032.
43. Kallenbach A. DIVERTOR ENRICHMENT OF RECYCLING IMPURITY SPECIES (HE, N2, NE, AR, KR) IN ASDEX UPGRADE. 29th IAEA Fusion Energy Conference; 16-21 Oct.; London, UK2023.
44. Henderson SS, Bernert M, Brida D, Cavedon M, David P, Dux R, et al. Divertor detachment and reattachment with mixed impurity seeding on ASDEX Upgrade. Nuclear Fusion. 2023;63(8):086024.
45. Field AR, Casson FJ, Fajardo D, Angioni C, Challis CD, Hobirk J, et al. Peripheral temperature gradient screening of high-Z impurities in optimised 'hybrid' scenario H-mode plasmas in JET-ILW. Nuclear Fusion. 2023;63(1):016028.
46. Dux R, Loarte A, Fable E, Kukushkin A. Transport of tungsten in the H-mode edge transport barrier of ITER. Plasma Physics and Controlled Fusion. 2014;56(12):124003.
47. Kallenbach A, Bernert M, Dux R, Reimold F, Wischmeier M, Team AU. Analytical calculations for impurity seeded partially detached divertor conditions. Plasma Physics and Controlled Fusion. 2016;58(4):045013.
48. Pitts RA, Bonnin X, Escourbiac F, Frerichs H, Gunn JP, Hirai T, et al. Physics basis for the first ITER tungsten divertor. Nuclear Materials and Energy. 2019;20:100696.
49. Freethy S, Figini L, Henderson M, El-Haroun H, Eliason B, Gibson S, et al. Microwave current drive for STEP and MAST Upgrade. EPJ Web Conf. 2023;277.
50. Wilson T, Freethy S, Henderson M, Köhn-Seeman A, Konoplev I, Saarelma S, et al. Electron Bernstein Wave (EBW) current drive profiles and efficiency for STEP. EPJ Web Conf. 2023;277.
51. Preinhaelter J, Pavlo P, Shevchenko V, Valovic M, Team M, Vahala L, et al. Electron Bernstein wave-X–O mode conversion and electron cyclotron emission in MAST. Review of Scientific Instruments. 2003;74(3):1437-40.
52. Luce TC, Lin-Liu YR, Harvey RW, Giruzzi G, Politzer PA, Rice BW, et al. Generation of Localized Noninductive Current by Electron Cyclotron Waves on the DIII-D Tokamak. Physical Review Letters. 1999;83(22):4550-3.
53. Farina D. A Quasi-Optical Beam-Tracing Code for Electron Cyclotron Absorption and Current Drive: GRAY. Fusion Science and Technology. 2007;52(2):154-60.
54. Freethy S. Microwave heating and current drive for STEP and MAST Upgrade. 29th IAEA Fusion Energy Conference; 16-21 Oct.; London, UK2023.
55. Biswas B. Fully relativistic EBW current drive simulations in STEP. 2024.
56. Harvey RW, McCoy MG. The CQL3D Fokker-Planck Code. 2015 1997. Contract No.: GA-A20978.
57. Mercier C. MHD stability criteria for localized displacements. Plasma Physics. 1979;21(7):589.
58. Jardin SC, Kessel CE, Menard J, Mau TK, Miller R, Najmabadi F, et al. Physics basis for a spherical torus power plant. Fusion Engineering and Design. 2003;65(2):165-97.
59. Kong M, Felici F, Sauter O, Galperti C, Vu T, Ham CJ, et al. Physics-based control of neoclassical tearing modes on TCV. Plasma Physics and Controlled Fusion. 2022;64(4):044008.
60. La Haye RJ, Buttery RJ, Gerhardt SP, Sabbagh SA, Brennan DP. Aspect ratio effects on neoclassical tearing modes from comparison between DIII-D and National Spherical Torus Experiment. Physics of Plasmas. 2012;19(6):062506.
61. Manickam J, Pomphrey N, Todd AMM. Ideal MHD stability properties of pressure-driven modes in low shear tokamaks. 1987 1987/03/01/. Report No.: PPPL-2420, 6460043.
62. Nasr E. Confining the Plasma - Magnetic Cage. Philosophicsl Transactions A 2024.
63. McClements KG, Hole MJ. Toroidal ripple transport of beam ions in the mega-ampère spherical tokamak. Physics of Plasmas. 2012;19(7):072514.
64. Ward SH, Akers R, Jacobsen AS, Ollus P, Pinches SD, Tholerus E, et al. Verification and validation of the high-performance Lorentz-orbit code for use in stellarators and tokamaks (LOCUST). Nuclear Fusion. 2021;61(8):086029.
65. Prokopyszen Aea. Confinement of fusion alpha-particles and Alfven eigenmode stability in STEP. Nucl Fusion. 2024.
66. Raman R, Shevchenko VF. Solenoid-free plasma start-up in spherical tokamaks. Plasma Physics and Controlled Fusion. 2014;56(10):103001-.
67. Kim H-T, Casson F, Meyer H, Cunningham G, Scannell R, Kogan L, et al. Development of full electromagnetic plasma burn-through model and validation in MAST. Nuclear Fusion. 2022;62(12):126012.
68. Erikkson F, Casson FJ, Challis CD, Baranov Y, Bakes S, Figini L, et al. Current ramp-up modelling for STEP. 48th EPS Conference on Plasma Physics; 27 June - 1 July; Maastricht, The Netherlands. europhysics conference abstracts: European Physical Society; 2022.
69. Mitchell J, Parrott A, Casson FJ, Eriksson FE, Koechl F, Lennholm M, et al. Scenario trajectory optimization and control on STEP. Fusion Engineering and Design. 2023;192:113777.
70. Sauter O, Angioni C. Neoclassical conductivity and bootstrap current formulas for general axisymmetric equilibria and arbitrary collisionality regime. Phys of Plasmas. 1999;6(7):2834-9.
71. Beurskens MNA, Angioni C, Bozhenkov SA, Ford O, Kiefer C, Xanthopoulos P, et al. Confinement in electron heated plasmas in Wendelstein 7-X and ASDEX Upgrade; the necessity to control turbulent transport. Nuclear Fusion. 2021;62(1):016015.
72. Xia G, Liu Y, Hender TC, McClements KG, Trier E, Tholerus E. Control of resistive wall modes in the spherical tokamak. Nuclear Fusion. 2023;63(2):026021.
73. Staebler GM, Kinsey JE, Waltz RE. A theory-based transport model with comprehensive physics. Physics of Plasmas. 2007;14(5):055909.
74. Pueschel MJ, Görler T, Jenko F, Hatch DR, Cianciara AJ. On secondary and tertiary instability in electromagnetic plasma microturbulence. Physics of Plasmas. 2013;20(10):102308.
75. Guttenfelder W, Candy J, Kaye SM, Nevins WM, Wang E, Bell RE, et al. Electromagnetic Transport from Microtearing Mode Turbulence. Physical Review Letters. 2011;106(15):155004.

76. Applegate DJ, Roach CM, Connor JW, Cowley SC, Dorland W, Hastie RJ, et al. Micro-tearing modes in the mega ampere spherical tokamak. Plasma Physics and Controlled Fusion. 2007;49(8):1113-28.
77. Giacomin M, Dickinson D, Kennedy D, Patel BS, Roach CM. Nonlinear microtearing modes in MAST and their stochastic layer formation. Plasma Physics and Controlled Fusion. 2023;65(9):095019.
78. Doerk H, Jenko F, Pueschel MJ, Hatch DR. Gyrokinetic Microtearing Turbulence. Physical Review Letters. 2011;106(15):155003.
79. Kennedy D, Giacomin M, Casson FJ, Dickinson D, Hornsby WA, Patel BS, et al. Electromagnetic gyrokinetic instabilities in STEP. Nuclear Fusion. 2023;63(12):126061.
80. Giacomin M, Kennedy D, Casson FJ, Dickinson D, Patel BS, Roach CM. Electromagnetic gyrokinetic instabilities in the Spherical Tokamak for Energy Production (STEP) part II: transport and turbulence. arXiv preprint arXiv:230701669. 2023.
81. Roach CM, Connor JW, Janjua S. Trapped particle precession in advanced tokamaks. Plasma Physics and Controlled Fusion. 1995;37(6):679-98.
82. Zohm H. Edge localized modes (ELMs). Plasma Phys Control Fusion. 1996;38:105-28.
83. Burrell KH, Austin ME, Brennan DP, DeBoo JC, Doyle EJ, Gohil P, et al. Quiescent H-mode plasmas in the DIII-D tokamak. Plasma Phys Control Fusion. 2002;44(5A):A253-A63.
84. Burrell KH, Barada K, Chen X, Garofalo AM, Groebner RJ, Muscatello CM, et al. Discovery of stationary operation of quiescent H-mode plasmas with net-zero neutral beam injection torque and high energy confinement on DIII-D. Physics of Plasmas. 2016;23(5):56103-.
85. Viezzer E, Austin ME, Bernert M, Burrell KH, Cano-Megias P, Chen X, et al. Prospects of core–edge integrated no-ELM and small-ELM scenarios for future fusion devices. Nuclear Materials and Energy. 2023;34:101308.
86. Harrer GF, Wolfrum E, Dunne MG, Manz P, Cavedon M, Lang PT, et al. Parameter dependences of small edge localized modes (ELMs). Nuclear Fusion. 2018;58(11):112001-.
87. Labit B, Eich T, Harrer GF, Wolfrum E, Bernert M, Dunne MG, et al. Dependence on plasma shape and plasma fueling for small edge-localized mode regimes in {TCV} and {ASDEX} Upgrade. Nuclear Fusion. 2019;59(8):86020-.
88. Faitsch M, Eich T, Harrer GF, Wolfrum E, Brida D, David P, et al. Analysis and expansion of the quasi-continuous exhaust (QCE) regime in ASDEX Upgrade. Nuclear Fusion. 2023;63(7):076013.
89. Bernert M, Janky F, Sieglin B, Kallenbach A, Lipschultz B, Reimold F, et al. X-point radiation, its control and an ELM suppressed radiating regime at the ASDEX Upgrade tokamak. Nuclear Fusion. 2021;61(2):024001.
90. Bernert M, Wiesen S, Février O, Kallenbach A, Koenders JTW, Sieglin B, et al. The X-Point radiating regime at ASDEX Upgrade and TCV. Nuclear Materials and Energy. 2023;34:101376.
91. Maingi R, Osborne TH, LeBlanc BP, Bell RE, Manickam J, Snyder PB, et al. Edge-Localized-Mode Suppression through Density-Profile Modification with Lithium-Wall Coatings in the National Spherical Torus Experiment. Physical Review Letters. 2009;103(7):075001.
92. Maingi R, Boyle DP, Canik JM, Kaye SM, Skinner CH, Allain JP, et al. The effect of progressively increasing lithium coatings on plasma discharge characteristics, transport, edge profiles and ELM stability in the National Spherical Torus Experiment. Nuclear Fusion. 2012;52(8):083001.
93. Imada K. Observation of new pedestal regime for MAST Upgrade H-mode plasmas. Nucl Fusion Letter. 2024.
94. Cathey A, Hoelzl M, Harrer G, Dunne MG, Huijsmans GTA, Lackner K, et al. MHD simulations of small ELMs at low triangularity in ASDEX Upgrade. Plasma Physics and Controlled Fusion. 2022;64(5):054011.
95. Meier L, Hoelzl M, Cathey A, Huijsmans G, Viezzer E, Dunne M, et al. MHD simulations of formation, sustainment and loss of quiescent H-mode in the all-tungsten ASDEX Upgrade. Nuclear Fusion. 2023;63(8):086026.
96. Ryan DA, Dunne M, Kirk A, Saarelma S, Suttrop W, Ham C, et al. Numerical survey of predicted peeling response in edge localised mode mitigated and suppressed phases on ASDEX upgrade. Plasma Physics and Controlled Fusion. 2019;61(9):095010.
97. Rosenbluth MN, Putvinski SV. Theory for avalanche of runaway electrons in tokamaks. Nuclear Fusion. 1997;37(10):1355-62.
98. Vallhagen O, Pusztai I, Hoppe M, Newton SL, Fülöp T. Effect of two-stage shattered pellet injection on tokamak disruptions. Nuclear Fusion. 2022;62(11):112004.
99. Tinguely RA, Izzo VA, Garnier DT, Sundström A, Särkimäki K, Embréus O, et al. Modeling the complete prevention of disruption-generated runaway electron beam formation with a passive 3D coil in SPARC. Nuclear Fusion. 2021;61(12):124003.
100. Hoppe M, Embreus O, Fülöp T. DREAM: A fluid-kinetic framework for tokamak disruption runaway electron simulations. Computer Physics Communications. 2021;268:108098.
101. Fil A, et.al. Disruption Runaway Electron generation and mitigation in STEP. Nucl Fusion. 2024.
102. Vallhagen O, Pusztai I, Helander P, Newton SL, Fülöp T. Drift of ablated material after pellet injection in a tokamak. Journal of Plasma Physics. 2023;89(3):905890306.
103. Berger E, Pusztai I, Newton SL, Hoppe M, Vallhagen O, Fil A, et al. Runaway dynamics in reactor-scale spherical tokamak disruptions. Journal of Plasma Physics. 2022;88(6):905880611.
104. Paz-Soldan C, Reux C, Aleynikova K, Aleynikov P, Bandaru V, Beidler M, et al. A novel path to runaway electron mitigation via deuterium injection and current-driven MHD instability. Nuclear Fusion. 2021;61(11):116058.
105. Hollmann EM, Baylor L, Boboc A, Carvalho P, Eidietis NW, Herfindal JL, et al. Trends in runaway electron plateau partial recombination by massive H ₂ or D ₂ injection in DIII-D and JET and first extrapolations to ITER and SPARC. Nuclear Fusion. 2023;63(3):036011.
106. Reux C, Paz-Soldan C, Aleynikov P, Bandaru V, Ficker O, Silburn S, et al. Demonstration of Safe Termination of Megaampere Relativistic Electron Beams in Tokamaks. Physical Review Letters. 2021;126(17):175001.
107. Battey AF, Hansen C, Garnier D, Weisberg D, Paz-Soldan C, Sweeney R, et al. Design of passive and structural conductors for tokamaks using thin-wall eddy current modeling. Nuclear Fusion. 2024;64(1):016010.
108. Izzo VA, Pusztai I, Särkimäki K, Sundström A, Garnier DT, Weisberg D, et al. Runaway electron deconfinement in SPARC and DIII-D by a passive 3D coil. Nuclear Fusion. 2022;62(9):096029.
109. Hornsby WA, Gray A, Buchanan J, Patel BS, Kennedy D, Casson FJ, et al. Gaussian process regression models for the

properties of micro-tearing modes in spherical tokamaks. Physics of Plasmas. 2024;31(1):012303.